Journal of Chromatography A, 1443 (2016) 201–210

Contents lists available at ScienceDirect

Journal of Chromatography A

journal homepage: www.elsevier.com/locate/chroma

Liquid chromatography coupled to tandem and high resolution mass spectrometry for the characterisation of ofloxacin transformation products after titanium dioxide photocatalysis

Javier Jimenez-Villarin[a,c], Anna Serra-Clusellas[b], Cristina Martínez[d], Aleix Conesa[b], Júlia Garcia-Montaño[b], Encarnación Moyano[c,*]

[a] Hidroquimia, C/de la Innovació, 2, 08225 Terrassa, Barcelona, Spain
[b] Leitat Technological Center, C/de la Innovació, 2, 08225 Terrassa, Barcelona, Spain
[c] Department of Analytical Chemistry, University of Barcelona, Diagonal 647, 08028 Barcelona, Spain
[d] Centro Tecnológico de Investigación Multisectorial (CETIM), Rúa As Carballeiras s/n, 15071, Edificio CICA, Campus de Elviña, A Coruña, Spain

ARTICLE INFO

Article history:
Received 11 December 2015
Received in revised form 21 March 2016
Accepted 21 March 2016
Available online 23 March 2016

Keywords:
Photocatalysis
Fluoroquinolones
LC-HRMS(MS/HRMS)
Data mining techniques

ABSTRACT

The characterization of pharmaceutical drugs and their transformation products have become an important analytical research field because its presence in the environment could induce bacterial resistance. Despite all efforts made by the scientific community, detection and structure identification of unknown chemicals still remains the most challenging task in non-targeted analytics. Given that, the objective of the present study was to develop an untargeted workflow to detect, quantify, identify and characterize ofloxacin and its transformation products (OFX TPs) after photocatalytic treatments based on TiO_2 nanoparticles and TiO_2 nanofibers. For the characterization and chemical structure assignment of OFX TPs, mass defect filters, mass accurate measurements (HRMS), tandem mass spectrometry in a q-Orbitrap (MS/HRMS) and the photocatalysis of the isotopically labelled ofloxacin (OFX-d_3) were used. Since a large set of data was obtained in each run, data treatment based on statistical analysis and mass defect filtering was used to reduce the number of potential TP candidates from 2497 m/z peaks to 70. Moreover, ions generated by in-source CID and by redox reactions in the electrospray source (ESI) were also detected and discarded from the TP candidate list. Moreover, the whole kinetics evolution of the generated TPs provided a deeper insight into the degradation mechanism and was used to propose a degradation pathway for the OFX in the aqueous phase. The time evolution of the TPs generated during the photocatalytic process using both types of catalysts (NPs and NFs) and different set-ups (suspended and supported conditions) indicated that OFX was completely removed from the aqueous solution in less than 4 h. Among the condition tested TiO_2 nanoparticles in suspended conditions showed the fastest kinetics (k: 0.161 min^{-1}).

1. Introduction

There is an increasing concern over antibiotics and its presence in the environment, since they and/or their metabolites could induce bacterial resistance. Among them, fluoroquinolones are a wide class of antibacterial agents used for human and veterinary applications. Conventional sewage treatment plants are not able to remove these chemicals, and as a result, they are being introduced into the aquatic environment at parts per-billion ($\mu g\,L^{-1}$) and parts per-trillion ($ng\,L^{-1}$) concentration levels. Although these concentrations are much lower than those used in medical applications, the related potentially toxic effects in the aquatic environment are still poorly known and cannot be discarded.

Heterogeneous photocatalysis is an advanced oxidation process (AOP) that can achieve complete oxidation and mineralisation of organic compounds [1–4]. The UV irradiation of the semiconductor promotes the formation of reactive oxidative species (ROS), which are able to destroy these chemicals to its complete degradation to CO_2 and H_2O [5–7]. TiO_2, ZnO and doped nanoparticles (with other metals or different semiconductors [8]), amongst others, have been extensively investigated as the suspended semiconductors in common heterogeneous photocatalysis set-ups [2–4]. However, the complete recovery of the semiconductor is still a major industrial challenge for its reutilisation. It is for this reason that heterogeneous

* Corresponding author at: Department of Analytical Chemistry, University of Barcelona, Av. Diagonal 647, 08028 Barcelona, Spain.
E-mail address: encarna.moyano@ub.edu (E. Moyano).

http://dx.doi.org/10.1016/j.chroma.2016.03.063
0021-9673/

photocatalysis, based on supported nanofibers, represents a great alternative to overcome this problem [9–11].

If the complete degradation of the pollutant is not achieved, the generated transformation products (TPs) may also promote microbial resistance, but its toxic effects are not known or have been little investigated. This task represents a particular analytical challenge because most of the by-products generated are new chemical entities, for which standards are not available. For the identification of these TPs, ultra high performance liquid chromatography (UHPLC) coupled to high-resolution mass spectrometry (HRMS) using electrospray ionization (ESI) is the analytical technique of choice since it makes it possible the measure of hundreds of TPs in a single full scan mass spectrometry analysis. The detection of these chemicals is a challenging task because the ions of interest are often masked by background noise or are coeluting with other ions of interest. In order to overcome this tedious task, data mining techniques such as mass defect filters (MDF) and isotopic pattern filters (IPF) are frequently used [12–14]. To characterise these new chemical entities, different approaches might be considered. The first option is to compare the measured MS/MS against tandem MS databases such as Metlin [15], Massbank [16] and more recently, MZCloud [17]. Nevertheless, the size and content of these databases are limited to a reduced number of known compounds. Another useful tool is the comparison of the measured MS/MS against *in silico* MS/MS spectra generated by different MS computational tools, such as MetFrag, Mass Frontier, ACD lab, amongst others [18–20]. Finally, new approaches, described in the metabolomics and proteomic literature, consisting of Hydrogen/Deuterium Exchange (HDX) [21–23] or Stable Isotope Labeling (SIL) techniques [24,25] can also be useful for the chemical structural elucidation of these TPs.

In this work we present a strategy for the detection and characterisation of ofloxacin (OFX) TPs to provide a deeper insight into its degradation pathway. Compared to previous photocatalytical studies of OFX [26–28] and other organic molecules [2–4] this work presents the adaptation and optimisation of in home data scripts (mass defect filters, isotope pattern matching, and other statistical tools) to overcome limitations in the detection and identification of these new chemical entities since their standards are not commercially available. Moreover, it is the first time that the photocatalysis of the deuterated ofloxacin (OFX-d_3) has been used to discriminate between positional isomers, and to provide an extra confirmation about the degradation mechanism.

2. Experimental

2.1. Chemicals and reagents

Ofloxacin (OFX), ofloxacin-d_3 (OFX-d_3) and TiO_2 P25-Degussa were purchased from Sigma-Aldrich (Steinheim, Germany). LC/MS grade acetonitrile and water were obtained from Fluka (Steinheim, Germany), while formic acid (98–100%) was purchased from Merck (Darmstadt, Germany). Individual OFX and OFX-d_3 stock solutions (1000 mg L^{-1}) were prepared in acetonitrile:water (1:1 *v/v*) and stored at −18 °C. Working standards were prepared by dilution in water from the stock solution. Nitrogen (99.995% pure) supplied by Air Liquide (Barcelona, Spain) was used as the sheath and auxiliary gas in the API source and as collision-induced dissociation gas (CID gas) in the MS/HRMS experiments.

2.2. Photocatalysis experiments

Photocatalytic experiments with artificial irradiation were performed in a 600 mL borosilicate 3.3 photochemical reactor (Trallero&Schlee, Barcelona, Spain). Photocatalytic experiments with suspended and supported TiO_2 P25 nanoparticles (NPs) or home-made TiO_2 nanofibers (NFs), synthetized by electrospinning, were carried out as follows: 350 mL of an aqueous solution containing 10 mg L^{-1} of OFX (or OFX-d_3) and the appropriate amount of TiO_2 NPs (or NFs) was added so as to have the desirable catalyst loading (250 mg L^{-1}). The resulting suspension was loaded into the photochemical reactor and sonicated for 30 min in darkness to ensure the homogenization of the TiO_2 suspension and the complete equilibration of adsorption/desorption of the substrate on the catalyst surface. The solution was then irradiated using 4 UVA lamps of 25 W (Radium Ralutec, 9W/78, 350–400 nm, λmax = 365 nm) placed around the reactor, providing a total UV irradiation at the center of the solution in the 0.8–1.1 mW cm^{-2} range. UV irradiation was measured with an UV light meter YK-35UV from Lutron (Barcelona, Spain). In photocatalytic experiments with supported TiO_2 (NPs or NFs), 10 mg of TiO_2 were supported on a glass fiber support and left at the bottom of the photochemical reactor. These experiments were carried out with 50 mL solution containing 10 mg L^{-1} OFX (or OFX-d_3), and one 25W UVA lamp (Radium Ralutec, 9W/78, 350–400 nm, λmax = 365 nm) placed above the reactor providing a total irradiance of 1.6 mW cm^{-2}. Three reference experiments were also carried out in the same experimental conditions: 10 mg L^{-1} OFX solution was maintained for 4 h without irradiation and without catalyst; 10 mg L^{-1} OFX solution was maintained for 4 h without irradiation but with catalyst and 10 mg L^{-1} OFX was irradiated without catalyst (photolysis). Temperature was kept at 25 ± 2 °C and the solution was stirred at 200 rpm in both set-up experiments. For safety considerations, a UV light mask was used for eye protection. To follow the kinetic evolution of photoproducts, 14 samples were periodically withdrawn from the reactor: 0, 5, 10, 15, 20, 25, 30, 60, 90, 120, 150, 180, 210 and 240 min.

2.3. Sample treatment

Sample aliquots (4 mL in suspended conditions and 400 μL in supported conditions) were stored at −70 °C until their analysis. Samples were centrifuged at 20,000*g* (15,000 rpm) for 15 min to remove catalyst particles in the experiments where TiO_2 was suspended. In supported photocatalysis, no sample pre-treatment was needed, as no catalyst was leeched from the filter to the solution. Prior injection, all samples were filtered through a 0.22 μm PVDF filter (Agilent, PaloAlto, CA, USA) and diluted (1:20) with LC–MS grade water before the HPLC-HRMS analysis.

2.4. High performance liquid chromatography

High performance liquid chromatography (HPLC) was performed on an Accela HPLC system (Thermo Fisher Scientific, San Joseí, CA, USA) equipped with a quaternary pump, an autosampler and a column oven. A BEH C18 column (100 × 2.1 mm and 2.5 μm particle size; Waters, Milford, MA, USA) was used with a flow rate of 400 μL min^{-1} and held at 40 °C. Solvents used in the gradient elution program were H_2O (solvent A) and CH_3CN (solvent B) both acidified with a 0.1% formic acid (*v/v*) when using positive ESI and H_2O (solvent A) and CH_3CN (solvent B) when applying negative ESI. In both cases, the gradient elution program was as follows: 10% B isocratic for 1 min as initial conditions, then in 5 min solvent B was risen up to a 90% B and this mobile phase composition was held for 1 min; finally the system went back to initial condition in 1 min.

2.5. High resolution mass spectrometry

HPLC-HRMS analysis was performed in a Q-Exactive Orbitrap (Thermo Fisher Scientific, San Joseí, CA, USA) equipped with a thermally assisted electrospray ionization source (H-ESI II). The operating parameters in positive mode were as follows: ESI

voltage was 3.5 kV; capillary and vaporizer temperatures were 320 °C; sheath gas, auxiliary gas and sweep gas flow rate were 40, 10 and 2 au (arbitrary units) respectively, and the tube lens was held at 50 V. In the negative mode, the ESI voltage was set at −2.5 kV and the rest of tune parameters were the same as in positive mode. In order to facilitate the ionisation in negative mode a 5 μL min^{-1} post column addition of NH_3 (0.25% *v/v*) was used. For targeted tandem MS experiments (MS/HRMS), nitrogen was used as collision gas (1.5 mTorr), and the normalized collision energy (NCE) ranged from 20 to 60% depending on the compound. The mass spectrometer was operated in profile mode (scan range, *m/z* 100–1000) with a resolving power of 70,000 FWHM (*full width half maximum*) (at *m/z* 200) and an automatic gain control setting of 3×10^6 with a maximum injection time of 200 ms.

2.6. Peak extraction

The generated *raw data files were converted to *mzXML files with the MSConverter software (http://proteowizard.sourceforge.net). These files were processed using MZmine version 2.3, an open source LC–MS derived data processing software (http://mzmine.sourceforge.net/). The accurate LC–HRMS data was imported and a list of ions for each scan was generated using the exact mass algorithm. All *m/z* values under a 10% relative intensity of each full scan spectrum were discarded for further data analysis. This step might be critical if a high threshold is chosen, since low abundance candidates would be missed. For each *m/z* value that could be detected continuously over ten scans, the extracted mass chromatogram was constructed and deconvoluted. To avoid peak duplication due to the isotopic pattern, M + 1 and M + 2 peaks were fitted into one candidate. Chromatograms were aligned using the RANSAC algorithm implemented in MZmine2. Maximum allowed retention time difference before the alignment was set to 0.3 min and maximum allowed retention time difference after the alignment process was set to 0.1 min. The software automatically calculated the number of iterations performed by the algorithm. Finally, each *m/z* extracted ion chromatogram was integrated across all samples.

2.7. Data analysis

Untargeted data treatment was processed using MATLAB 2014a (Mathworks, Natick, MA, USA) with home-made scripts. Data analysis was performed in two steps. The first step was the selection of potential TPs based on three criteria: 1) the LC-HRMS peak should be detected in two consecutive points during the kinetic experiments, 2) the peak area should be above a threshold value of 10^5 units, 3) the candidate ion should present a linear response when diluting. To check the response linearity of the different candidates, samples were diluted 10 times and 100 times. If this requirement was not accomplished, the *m/z* value was removed despite having passed the first two filters. The second step in data analysis included the evaluation of a multiple mass defect and isotopic patterns (using 3 isotopes) filters. For the selected candidates, its molecular formulae was estimated with a mass tolerance of 5 ppm within the following composition ranges: $C_{(5-40)}$, $H_{(10-60)}$, $O_{(0-10)}$, $N_{(0-8)}$ and $F_{(0-3)}$.

Structural elucidation was based on the accurate mass of the selected candidates and their product ion scan (MS/HRMS). Identification of degradation products was confirmed when possible by direct comparison to on-line databases of the obtained HRMS and MS/HRMS and in-silico fragmentation prediction.

3. Results and discussions

In this work, analytical tools based on LC-ESI-HRMS and data-mining techniques were adapted and optimised for a high throughput in the detection and structural elucidation of OFX TPs after a photocatalytical treatment based on TiO_2 nanoparticles and nanofibers. The photocatalytic degradation of the deuterated homologue, OFX-d_3 ($\Delta m/z$ 3.0188), was also carried out in order to support the structural elucidation of the identified TPs. The LC-HRMS raw files were imported to MZmine2 for peak extraction and then exported to MATLAB for further data evaluation. Statistical evaluation and multiple mass defect filtering were essential to significantly reduce the original data set of more than 2000 *m/z* peaks to 134 potential signals to be considered as OFX TPs. Only those signals appearing in OFX and OFX-d_3 photocatalysis at the same retention time were finally considered for further studies, thus reducing the generated list to 70 potential TP candidates. After testing different instrumental conditions, ion generated by in-source CID and redox reactions were obviated and the potential TP list was further reduced to 59. Since no standards are available to unambiguously identify and confirm the identity of the generated TPs, HRMS in the full scan mode and target MS/HRMS in combination with the isotopically labelled OFX were used to provide structural evidences on the nature of these ions detected. Deuterated ofloxacin not only proved to be useful in order to annotate possible structures given a molecular formulae, but also in terms of understanding the mechanism and the degradation pathway involved in the photocatalytical process of these kind of organic compounds. Although ESI in the negative ionisation mode was also studied no complementary or significant data was obtained in this ionisation mode. Regarding the quantitative analysis, given the lack of standards, the wide range of photoproducts generated during the photocatalytical process, and thus, not knowing the response factor for these compounds, a semi-quantitative approximation was performed with the extracted peak area of each individual transformation product.

3.1. Data analysis

The extracted raw data was arranged into an $m \times n$ peak matrix, where *m* was the set of samples analysed (12) and *n* was the set of ions detected (*m/z* values) in each sample (2497). After the application of the first data analysis step described in the Section 2, a total of 2270 background ions were removed from the original peak list, obtaining a new matrix of 12×227. The second step in data evaluation, which was based on the chemical structure, consisted in the application of a single (SMDF) and multiple (MMDF) mass defect filters that were developed, applied and compared using in home-scripts. The SMDF was based on the core structure of ofloxacin and common reactions that can take place during the photocatalytical process: multiple hydroxylation/dehydroxylation (±n OH; ±n 2.7 mDa), CO_2 loss (10.17 mDa), defluorination (−1.6 mDa), C—C oxidations/reductions (±n H_2; ±n 15.66 mDa). It is for that reason that SMDF was chosen to be between 100 and 200 mDa over the mass range of 300–400 Da. As a result, only 35 candidates with closely related chemical structure to OFX were identified as potential TPs. Moreover, the previous inspection of the raw LC-HRMS data also revealed the presence of ions at *m/z* below 300 and over 500, in agreement to previous works reported by Hapeshi et al. [27], Michael et al. [28] and Hapeshi et al. [29]. For instance, these authors reported the cleavage of the piperazine ring of OFX yielding the $[M+H]^+$ ion at *m/z* 279 and the dimerisation of the OFX molecule generating the $[M+H]^+$ ion at *m/z* 588. Hence, a MMDF was developed in order to consider TPs over the whole mass range. In addition to the SMDF (Filter #1 of the MMDF), Filter #2 was chosen to be around a mass defect of 50–100 mDa covering a mass range of 200–300 Da; Filter # 3 was chosen to be between 500 and 700 Da comprising a mass defect between 450 and 550 mDa in order to output dimers and high molecular weight structures. When the MMDF was applied, 99 OFX TPs were identified in addition to those 35

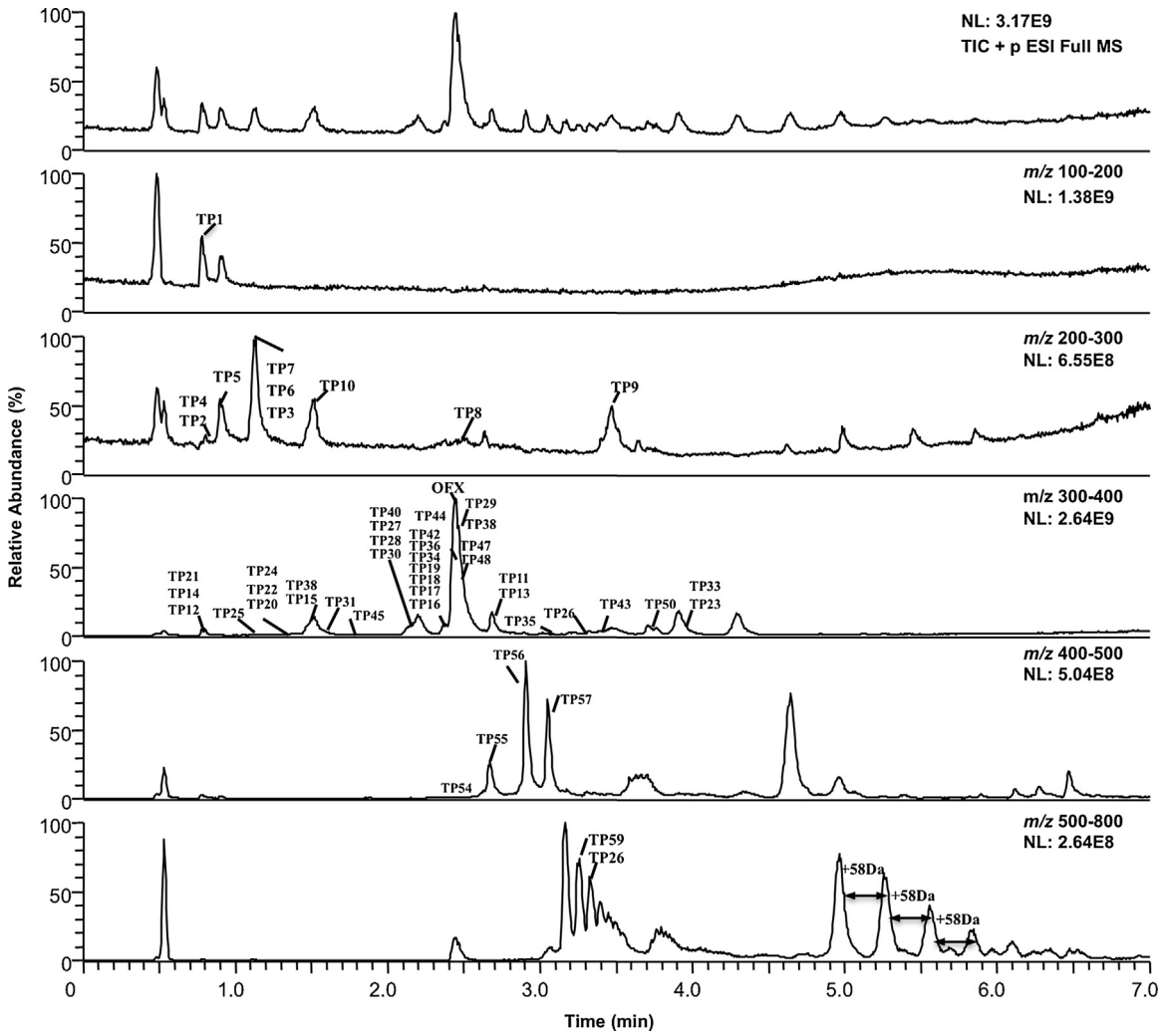

Fig. 1. (A) Total ion chromatogram in the electrospray positive ion mode m/z 100–1000 is shown for a sample collected at 15 min under supported TiO_2 nanofibers (B) m/z 100–200; (C) m/z 200–300; (D) m/z 300–400; (E) m/z 400–500 and (F) m/z 500–800. Characteristic retention time of all TPs detected is shown in the presented chromatograms.

candidates obtained with the SMDF. For the best filtering performance, the MMDF had to be applied as no good results were obtained by extending the SMDF algorithm (increasing m/z and mass defect ranges). Fig. 1 shows the TIC and extracted ion chromatograms in different m/z ranges in order to illustrate how extensive the generation of TPs was. After the whole process of data analysis mentioned before, this 12×134 matrix was further reduced by only picking up those signals appearing in OFX and OFX-d_3 photocatalysis. Every MS scan was inspected for pairs of two m/z peaks, M, which corresponded to OFX TPs, and ($M + n \times 3.0188$ Da, being n the number of $-CD_3$ groups) which denoted OFX-d_3 TPs. The acceptance criteria for each pair of m/z peaks were a maximum mass tolerance (1 ppm) and a maximum allowed retention time of 0.2 min. Thus, a comprehensive list of 70 candidate ions was obtained, being reduced to 59 candidates after discarding those ions generated by both in-source CID and redox reactions, as described in Section 3.2. Table 1 summarises the final list, showing the accurate m/z value identified, the proposed molecular formula and its associated mass relative error (ppm), RDB (ring and double bond equivalents), the isotopic pattern fit and retention time (minutes). The accurate mass measurement and the product ion mass spectra of OFX and its TPs were used to elucidate and to propose a tentative chemical structure. Data compiled in Table S1 shows the most characteristic product ions, their experimental m/z value, associated mass relative error (ppm), ion assignment and RDB value).

3.2. Discrimination between TPs and in-source generated ions

Different operational conditions should be tested when conducting untargeted analysis, especially if the nature of the analytes under study is not known or has not been previously studied. In order to discard those ions originated by in-source fragmentation, adduct formation or redox reactions in the ESI source, the effect of the electrospray working conditions were studied. Two different samples submitted to the photocatalysis process with TiO_2 NPs and TiO_2 NFs were chosen for this purpose.

3.2.1. In-source CID fragmentation and adduct formation

The S-lens and in-source fragmentation energy are tune parameters that can favour in-source CID fragmentation. For that reason, these parameters were changed in replicated injections between 40 and 80 V and between 5 and 50 eV respectively. Two coeluting candidates (2.50 min) to be TPs, both detected in the positive ESI mode, m/z 360.1356 and m/z 378.1463, were checked for the in-source CID fragmentation. The absence of the product ion at m/z 360.1356 in the MS/MS spectrum of the ion at m/z 378.1463 confirmed the independent nature of both ions. Another in-source CID fragmentation example was found for m/z 318.1610, which showed two chromatographic peaks at 2.48 and 2.68 min, the last one at the same retention time of OFX. Both m/z signals were attributed to the carbon dioxide cleavage from ofloxacin. The first peak (2.48 min)

Table 1
Detected ofloxacin transformation products after TiO_2 – NF photocatalysis. Deuterated molecular weights are not show.

TP	*m/z*	Molecular formula	Mass error (ppm)	RDB	Isotopic pattern fit (%)	Retention time (min)
1	195.1229	$[C_8H_{19}O_5]^+$	−1.3	−0.5	92	0.92
2	209.1018	$[C_8H_{17}O_6]^+$	0.6	0.5	95	0.90
3	217.1068	$[C_{10}H_{17}O_5]^+$	0.9	2.5	90	1.13
4	231.0832	$[C_5H_{14}N_2O_8]^+$	3.7	−0.5	91	0.89
5	254.1600	$[C_{10}H_{24}NO_6]^+$	0.8	−0.5	89	0.96
6	261.1035	$[C_{14}H_{14}FN_2O_2]^+$	0.4	8.5	96	1.15
7	275.1096	$[C_7H_{19}N_2O_9]^+$	4.0	−0.5	93	1.21
8	279.0776	$[C_{13}H_{12}FN_2O_4]^+$	0.1	8.5	94	2.55
9	279.0776	$[C_{13}H_{12}FN_2O_4]^+$	0.1	8.5	94	3.64
10	283.1756	$[C_{12}H_{27}O_7]^+$	1.7	−0.5	88	1.51
11	304.0928	$[C_{14}H_{14}N_3O_5]^+$	−0.1	9.5	90	2.70
12	305.0943	$[C_{15}H_{14}FN_2O_4]^+$	3.6	9.5	91	0.90
13	306.1083	$[C_{14}H_{16}N_3O_5]^+$	−0.5	8.5	91	2.80
14	314.0668	$[C_{13}H_{13}FNO_7]^+$	−0.8	7.5	90	0.90
15	315.1788	$[C_{11}H_{27}N_2O_8]^+$	−1.0	−0.5	93	1.61
16	316.1452	$[C_{17}H_{19}FN_3O_2]^+$	−1.0	9.5	88	2.48
17	318.1610	$[C_{17}H_{21}FN_3O_2]^+$	−0.6	8.5	89	2.48
18	319.1366	$[C_{12}H_{21}N_3O_7]^{+All\bullet}$	−2.3	4.0	95	2.31
19	320.1242	$[C_{15}H_{18}N_3O_5]^+$	0.2	8.5	91	2.34
20	329.1700	$[C_{15}H_{25}N_2O_6]^+$	−2.0	4.5	94	1.40
21	331.2102	$[C_{15}H_{29}N_3O_5]^{+\bullet}$	−0.4	3.0	94	0.90
22	334.1194	$[C_{16}H_{17}FN_3O_4]^+$	−1.0	9.5	91	1.40
23	335.1119	$[C_{15}H_{17}N_3O_6]^{+\bullet}$	2.2	9.0	90	3.94
24	336.1354	$[C_{16}H_{19}FN_3O_4]^+$	−0.1	8.5	93	1.40
25	338.1511	$[C_{16}H_{21}FN_3O_4]^+$	0.2	7.5	91	1.12
26	679.5114	$[C_{36}H_{67}N_6O_6]^+$	−0.7	6.5	91	3.35
27	340.2595	$[C_{18}H_{34}N_3O_3]^+$	−0.1	3.5	90	2.10
28	341.1216	$[C_{14}H_{19}N_3O_7]^{+\bullet}$	−0.5	7.0	90	2.33
29	342.2149	$[C_{17}H_{30}N_2O_5]^{+\bullet}$	−0.1	4.0	84	2.52
30	344.1609	$[C_{18}H_{21}N_3O_4]^+$	1.3	9.5	83	2.15
31	345.1884	$[C_{15}H_{27}N_3O_6]^{+\bullet}$	−3.0	4.0	85	1.61
32	346.1202	$[C_{17}H_{17}FN_3O_4]^+$	0.4	10.5	92	2.48
33	347.2048	$[C_{15}H_{29}N_3O_6]^{+\bullet}$	−0.7	3.0	93	3.90
34	348.1354	$[C_{17}H_{19}FN_3O_4]^+$	−0.1	9.5	95	2.48
35	349.1831	$[C_{14}H_{23}N_3O_7]^{+\bullet}$	−3.5	3.0	86	3.11
36	350.1146	$[C_{16}H_{17}FN_3O_5]^+$	+0.1	9.5	91	2.37
37	353.1718	$[C_{14}H_{26}FN_2O_7]^+$	−0.1	2.5	87	3.28
38	360.1356	$[C_{18}H_{19}FN_3O_4]^+$	0.2	10.5	90	1.62
39	360.1356	$[C_{18}H_{19}FN_3O_4]^+$	0.2	10.5	89	2.50
OFX	362.1510	$[C_{18}H_{21}FN_3O_4]^+$	−0.1	9.5	99	2.50
40	363.1549	$[C_{15}H_{24}FN_2O_7]^+$	−3.4	4.5	89	2.28
41	363.1629	$[C_{14}H_{25}N_3O_8]^{+\bullet}$	−1.8	4.0	85	2.15
42	364.1301	$[C_{17}H_{19}FN_3O_5]^+$	−0.2	9.5	86	2.25
43	364.1503	$[C_{17}H_{22}N_3O_6]^+$	−0.1	8.5	94	3.45
44	364.1671	$[C_{18}H_{23}FO_4N_3]^+$	0.4	8.5	91	2.40
45	365.1578	$[C_{17}H_{23}N_3O_6]^{+\bullet}$	−0.8	8.0	87	1.90
46	374.1149	$[C_{18}H_{17}FN_3O_5]^+$	0.3	11.5	93	2.48
47	376.1303	$[C_{18}H_{19}FN_3O_5]^+$	−0.1	10.5	91	2.50
48	378.1463	$[C_{18}H_{21}FN_3O_5]^+$	0.3	9.5	84	2.50
49	379.1510	$[C_{15}H_{24}FN_2O_8]^+$	−0.4	4.5	85	1.93
50	379.1497	$[C_{18}H_{23}N_2O_7]^+$	−0.8	8.5	80	3.81
51	392.1253	$[C_{18}H_{19}FN_3O_6]^+$	0.2	10.5	92	2.45
52	394.1411	$[C_{18}H_{21}FN_3O_6]^+$	0.5	9.5	83	2.45
53	396.1566	$[C_{18}H_{23}FN_3O_6]^+$	0.3	8.5	92	2.68
54	412.1521	$[C_{18}H_{23}FN_3O_7]^+$	1.6	8.5	81	2.51
55	430.1773	$[C_{22}H_{25}FN_3O_5]^+$	1.3	11.5	85	2.82
56	434.2087	$[C_{22}H_{29}FN_3O_5]^+$	0.2	9.5	88	2.94
57	447.2930	$[C_{19}H_{39}N_6O_6]^+$	0.8	12.0	80	3.08
58	505.3344	$[C_{22}H_{25}N_6O_7]^+$	−1.8	3.5	89	4.70
59	621.4221	$[C_{33}H_{57}N_4O_7]^+$	−0.1	7.5	95	3.24

was attributed to a TP generated in the photocatalysis process, while the other, eluting at 2.68 min was thought to be generated by in-source CID from OFX. This hypothesis was in accordance to the MS/HRMS fragmentation pattern of OFX, which yielded a product ion due to the CO_2 loss (*m/z* 318.1610). This fact was further confirmed by increasing the CID energy, which produced simultaneously a decrease on the intensity of protonated OFX $[M+H]^+$ and the increase in the abundance of *m/z* 318.1610. In addition to the mentioned examples, 5 additional suspect ions were found to be generated via in-source fragmentation, all being removed from the candidate list. Finally, this list was examined regarding for adduct formation (mainly H_2O, CH_3CN, HCOOH) in both positive and negative electrospray polarities. The absence of ions that matched in both retention times and mass shifts indicated that no adducts were present.

3.2.2. In-source oxidation

Redox reactions may occur in the ESI source [31] leading to false data interpretation. In these experiments, the ESI potential was varied between 2 and 4 kV to discriminate between those ions generated during the photocatalysis process from those that could be originated by a redox process in the ionisation source. For

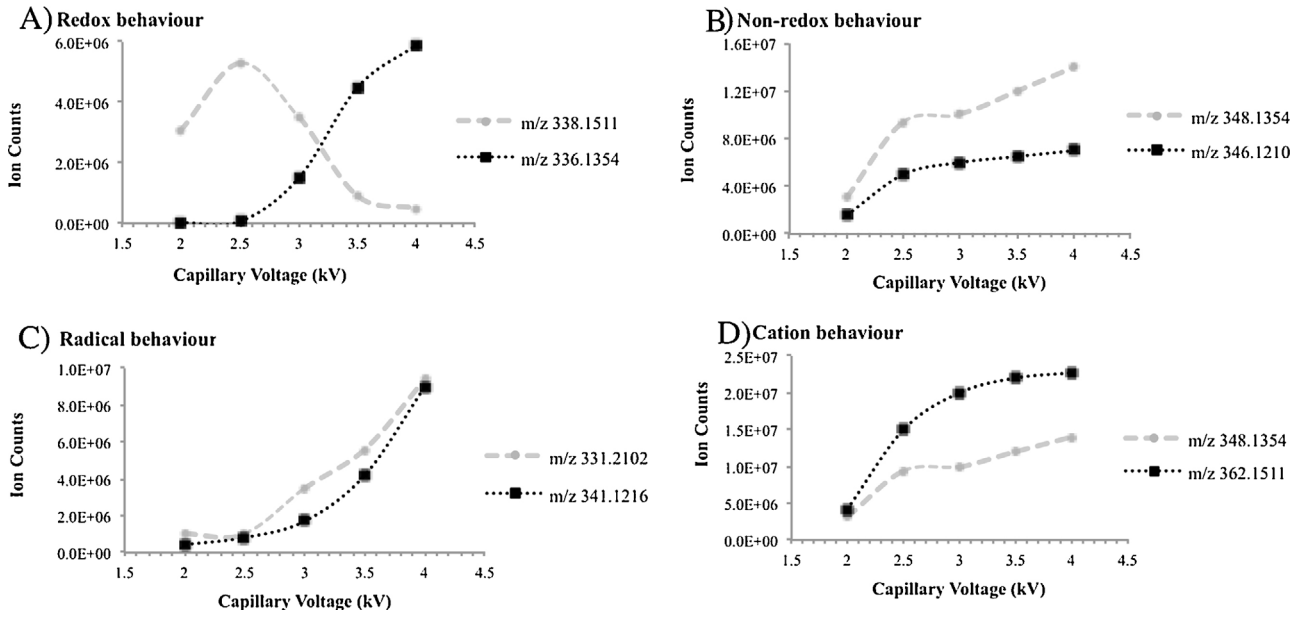

Fig. 2. Ion intensity behaviour *versus* the capillary voltage to illustrate: (A) Redox; (B) non-redox; (C) radical; (D) cation behaviours.

instance, the relative intensities of ions at *m/z* 336.1354 (t_R: 1.12 and 1.40) and *m/z* 338.1511 (t_R: 1.12 min) were recorded *versus* the ESI voltage in the positive mode (Fig. 2A). When the ESI voltage was gradually increased, the relative intensity of ion at *m/z* 336.1354 increased while the intensity of *m/z* 338.1511 simultaneously decreased when the ESI voltage was set over 2.5 kV. These results indicated that the first *m/z* peak could came from an oxidation process of *m/z* 338.1511, resulting in the oxidation of one hydroxyl group to carbonyl. In contrast, those ions not suffering redox reactions in the source only showed a slightly increase with the ESI voltage, as shown in Fig. 2B, with *m/z* 346.1210 and *m/z* 348.1354 respectively. In this study, other examples of redox reactions were found in the positive ionisation mode. Ions corresponding to TP21 and 28 (*m/z* 331.2102 and *m/z* 341.1216 respectively), which were considered to be radical cations ($[M]^{+\bullet}$) generated in the electrospray source, described a convex exponential function when the ESI voltage was gradually changed (Fig. 2C). Different to the mentioned behaviour, TP34 and OFX (*m/z* 348.13541 and *m/z* 362.15106 respectively, both $[M+H]^+$) showed a concave function when the ESI voltage was increase, represented in Fig. 2D. A total of eight radical cations (including the mentioned examples) were found to describe the same convex trend when the capillary voltage was changed.

3.3. Characterisation of ofloxacin transformation products

As mentioned in Section 3.1 and as can be seen in Fig. 1, 59 intermediates were identified as OFX TPs generated during the photocatalytical process. The elemental composition was calculated on the basis of the accurate *m/z* values and the isotopic patterns. For each TP, a chemical structure was proposed taking into account their high resolution product ion spectrum (MS/HRMS). Table S1 summarizes the MS/HRMS information of the most relevant TPs of OFX and OFX-d_3. Moreover, tentative chemical structures have been proposed for each TP after the interpretation of the mass spectral data obtained in this study and they have been also included in Table S1.

The first TPs to be characterised were those TPs sharing the same core structure of OFX and showing similar fragmentation patterns. For instance, TP 36, 39, 42, 51, 52, amongst others, showed the loss of H_2O (*m/z* 18.0105) due to one or multiple hydroxyl groups in their structure due to the attack of the radical OH. For instance, TP 48 was attributed to the hydroxylation at position 12, which was previously reported by Calza et al. [26]. Amongst the different positional isomers that could be hypothesized for TP48, position 12 is the only one able to show a water loss on TP48 and those TPs derived from it, that is, TP 46, 47, 51 and 52. Since the MS/MS spectrum of TP46, attributed to the hydroxylation at position 12 and oxidation at the pyperazine moiety, showed the same product ions of TP48, made it possible to discard the hydroxylation at position 2′ or 3′. Moreover, the •OH attack at position 14 was also discarded as it would have shown the loss of $C_3H_7NO_2$ on the quinolone moiety, as stated by Calza et al. The neutral loss of CO_2 (*m/z* 43.9898) was always observed in the MS/MS spectrum when the generated transformation products still had the quinolone moiety unmodified or with little modifications (TP 22, 23, 24 and 25 as well as TP 30–39). Additionally, the simultaneous loss of CO_2 and C_3H_7N occurring at the pyperazine moiety yielding the ion at *m/z* 261.1035 was observed in the MS/MS spectra of TPs 32, 34, 43 and 46, as well as in the tandem mass spectrum of OFX. The loss of C_3H_7N at the pyperazine moiety observed for OFX was of special significance since C—C oxidations of some of the generated TPs could be easily distinguished. For example, TPs 46–48 are a clear example on how this product ion could reveal how many unsaturations showed the pyperazine moiety, since the most unsaturated ring (3 unsaturations) showed the loss of C_3HN while the reduced form showed the loss of C_3H_7N (1 unsaturation). That was applicable to all TPs which showed oxidations in the piperazine ring.

Despite having obtained relevant data to characterise and attribute chemical structures to the identified TPs, the chemical structure of some of them could not be fully characterised. The information obtained with the accurate mass and the MS/HRMS was not enough relevant to propose a chemical structure with a high degree of confidence. Moreover, the lack of standards or previous literature describing such degradation made more complicated this characterisation. However, these transformation products were attributed to the lasts steps of ofloxacin degradation since they started appearing at the middle-end of the reaction. It is for this reason that TP1 to TP5 and TP10 could be the result of extensive hydroxylation and chemical transformations involving all chemical processes taking place during the photocatalytical treatment.

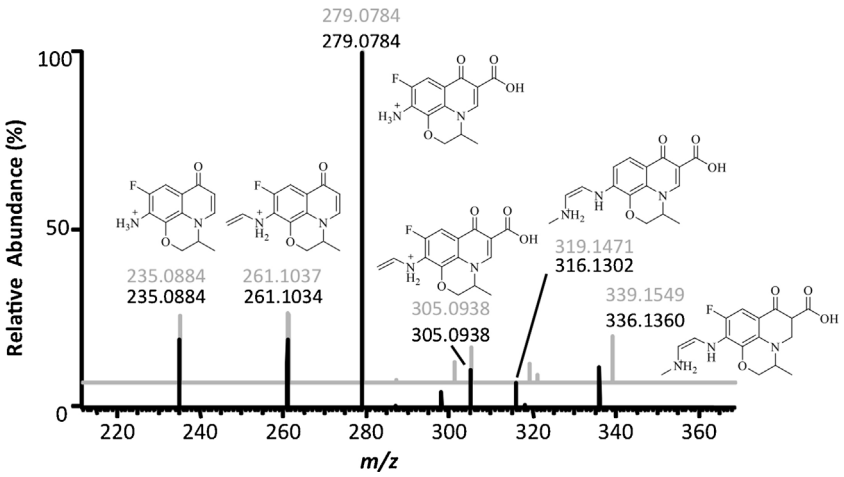

Fig. 3. MS/MS spectrum of non-deuterated (in black) and deuterated (in grey) of TP 24.

The comparison of the product ion spectra of TPs generated from the photocatalysis of OFX and OFX-d_3 was useful for the chemical structure assignment. Especially useful was when it was needed to know the tentative position of the different methyl groups present in the suspect molecule. Since the accurate m/z value can led to different molecular formulae, and thus, different molecular structures, the use of the deuterated ofloxacin (isotopically labelled in the piperazine methyl group) and target MS/HRMS (described in the Section 2) were crucial to discriminate amongst all possibilities. There are several examples in which the molecular structure was confirmed by means of the deuterated compound, that is, when the piperazine methyl did not suffer any modification. For instance, Fig. 3 shows the MS/HRMS spectra obtained for TP 24 (m/z 336.1360; m/z 339.1549) when studying both OFX and OFX-d_3 photocatalysis. After the opening of the piperazine ring and the likely loss of C_2H_4, the labeled methyl group, at 4′, still remained in this position, fact which lead to the proposal of the molecule shown in Fig. 3. Having applied the described methodology and reasoning, it was possible to confirm 18 structures generated after the photocatalysis process. On the other hand, if the same ions were observed in both experiments would indicate the loss of the piperazine methyl group or its substitution in the mentioned position. This was the case found for the rest of molecules presented in Table 1. Moreover, multiple potential deuterated molecules (n × 3.0188 Da) were inspected and were not detected. This would indicate that after radical CH_3/CD_3 loss, further methyl additions might not been taking place to the generated TPs. Moreover, the generation of dimers did not led to multiple deuterated molecules, thus indicating that the loss of the piperazine methyl is a previous step to molecule dimersisation or after the dimersisation of OFX or generated TPs, methyl groups are lost. However, despite all efforts made in this study, there is still a need to achieve higher confidence in the proposal of some chemical structures, since some identified isomers were not possible to distinguish on the basis of their accurate mass and their MS/MS pattern.

3.4. Degradation pathway

The OFX concentration over the photocatalytical process was monitored by LC-HRMS following the $[M+H]^+$ trace. Results were fitted into a first order kinetics and pseudo-constant rates obtained are shown in Table 2 for both suspended and supported experiments using TiO_2 nanoparticles and nanofibers. As it was expected, the degradation was faster when NPs or NFs were suspended in the media than under in supported conditions: as this higher rate can be attributed to the more available specific surface area to be in contact with the solution containing OFX. Similarly, TiO_2 NPs were able to achieve complete OFX removal faster than TiO_2 NFs due to its higher specific surface area.

Table 2
Pseudo-constant rates (min^{-1}) found for ofloxacin photocatalysis in the different tested conditions. A reference solution was also analysed without being submitted to irradiation. Photolysis blanks tests were also conducted in both set-ups tested.

	Suspended k (min^{-1})	r^2	Supported k (min^{-1})	r^2
Reference solution	–	–	–	–
Photolysis	0.007	0.98	0.023	0.95
TiO_2 P25	0.161	0.99	0.023	0.99
TiO_2 NF	0.022	0.97	0.032	0.95

Apart from the mentioned degradation rate, some differences in the TPs nature were found when comparing both materials. Independently of performing the experiment in suspended or supported conditions, low molecular weight TPs were observed when NPs were used, while NFs generated ions with higher m/z ratios. These differences observed in the TPs production suggested different degradation mechanisms when using NPs or NFs. However, due to the complexity of the photocatalytical process, these different mechanisms are still not known and they are under investigation.

After annotation of the candidate structures, two approximations were taken into account in order to suggest the path by which OFX is degraded: time evolution and mass comparison of all TPs generated from both OFX and OFX-d_3 photocatalysis in the different conditions tested. As no standards were available, peak area evolution has been considered, as in previous publications [26–34], as a quantitative approximation in order to follow the evolution of the generated TPs. The degradation pathway was built up looking for first-generation TPs, that is, small transformation changes to OFX structure. Then, consecutive degradation was investigated looking for small modifications to first-generation TPs. Most of these found TPs were characterised by maintaining the quinolone moiety, which is the main responsible for the antibacterial activity, thus, the drug is not inactivated [26–29].

A tentative degradation pathway is shown in Fig. 4. For instance, it was considered to be first generation TPs demethylation of the pyperazine ring (TP 34) yielding the ion at m/z 348.1354, hydroxyl attack and consecutive demethylation generating a hydroxylamine at the *N*-pyperazine position giving raise to TP 42 (m/z 364.1503), defluorination (TP 30) yielding the ion at m/z 344.1609, decarboxilation generating TP 17 (m/z 318.1610) and C_2H_4 loss at the 5′–6′ positions of the pyperazine ring yielding TP 24 (m/z 336.1354). Additionally, hydroxyl attack to the OFX quinolone moiety led to TP 48 (m/z 378.1463). The results from the extracted-ion chro-

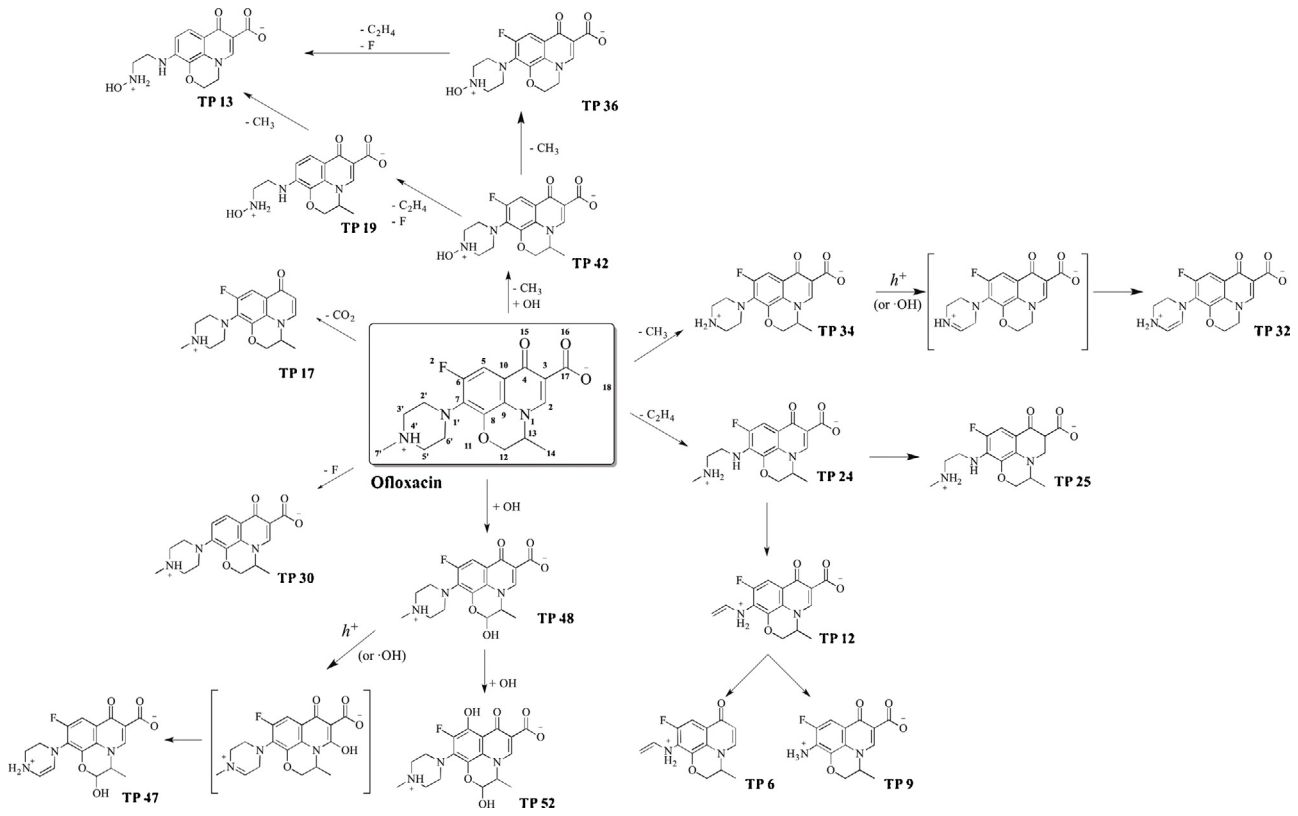

Fig. 4. Tentative degradation pathway of ofloxacin. Not all TPs detected and listed in Table 1 are shown.

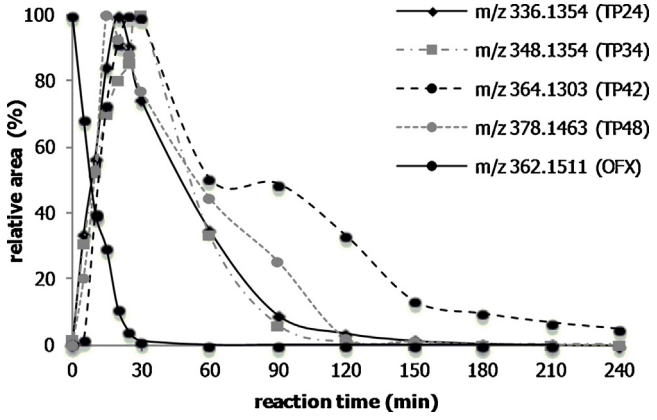

Fig. 5. Degradation kinetics of OFX (*m*/*z* 362.1511 in black dots), TP 24 (*m*/*z* 336.1354 in black diamonds), TP 34 (*m*/*z* 348.1354 in grey squares), TP42 (*m*/*z* 364.1303 in black dots and dashed lines) and TP 48 (*m*/*z* 378.1463 in grey dots).

matograms were handled to build plots of the TPs peak area evolution (% relative to their maximum) versus reaction time (Fig. 5). These TPs showed a fast concentration increase after 5 min of photocatalytical treatment, which agrees to the assumption of being first-generation TPs.

On the basis of time evolution and chemical reactions taking place during the photocatalyc process, consecutive degradation of these TPs occurred, and thus, next generation TPs were tentatively proposed. For instance, TP 24 could presumably lead to TP12 after the cleavage of the N—CH_2 bond between the 3′–4′ positions. Finally, TP 12 would tentatively lead to TP 6 (*m*/*z* 261.1035) and TP 9 (*m*/*z* 279.0776) after CO_2 and C_2H_4 loss respectively. TP 48 has been reported[25] to lead to TP 52 (*m*/*z* 394.1411) after the consecutive addition of a hydroxyl group to the quinolone moiety. TP 42 could presumably lead to TP 36 (*m*/*z* 350.1146) and TP 19 (*m*/*z* 320.1242) after the loss of the methyl group and the simultaneous loss of −F and C_2H_4 (5′–6′) respectively. These last two mentioned TPs could explain the generation of TP 13 (*m*/*z* 306.1083) via two different reaction mechanisms. In regard to the faster concentration increase of TP 36 (Fig. S1), the loss of the methyl group at position 13 seems to be favoured in comparison to the loss of C_2H_4 in the pyperazine ring. Also this was confirmed by knowing at which kinetic point both TPs started to appear, thus, being 10 min for TP 36 and 20 min for TP 19. However, parallel reaction pathways leading to the same TP may also be considered, as for example, TP 19 showed a concentration increase after 120 min of treatment.

Apart from oxidation due to reactive oxidative species (ROS), the generated holes (h^+) on the TiO_2 surface (Fujishima et al. and Salvador) can also oxidate organic species if they are adsorbed on the surface of the catalyst. A tentative explanation rationalising its presence has been reported in previous literature [36] and the mechanism for this particular case is shown in Fig. S2. After an electron capture by the N atom at the 1′ or 4′ and consecutive electron rearrangement, a new N—C bond might be formed leading to an imine or an iminium ion. These compounds might immediately be transformed to their respective enamines after losing the H at position 6′ thus appearing TPs 16, 22, 32, 39, 47 and 51 or the pyperazine ring might be opened leading to different reactions.

Although not being the most common reactions in TiO_2 pohotocalysis, reduction processes occurring at the quinolone moiety were also observed on some of the identified TPs, for instance TP 24 to TP25 or OFX to TP44. These reduction processes have been previously reported in literature [33,35]. The interaction of H^+ ions with the excited electrons, generated after the emission of one electron from the valence band to the conduction band, leads to the formation of $H^\bullet$ radicals and molecular hydrogen at the photocatalyst's surface, thus being plausible these reduction processes on the mentioned molecules.

High molecular weight molecules (m/z 500–1000) were separated on the C18 LC column as shown in Fig. 1. The presence of such molecules has been extensively reported [29,34]. The stabilized organic radicals can be subject to dimerization reactions via carbon–carbon or carbon-oxygen couplings or via addition of such radicals onto neutral molecules [33]. Structure annotation of some of these signals was not possible due to the fact that tandem MS was not obtained despite having performed different LC runs increasing the collision energy. However, it was noticed a mass difference of +58 Da between consecutive chromatographic peaks indicated in Fig. 1, which could be attributed to consecutive additions of butyl groups. There were some exceptions, as TP 26 (m/z 679.5181, (m/z 340.2591 due to $[M+2H]^{2+}$)) shown in Fig. S4, which tentatively resulted from the condensation of two core structures of ofloxacin and the consecutive groups cleavage and oxidation/reductions reactions, as it was observed in previous examples shown in Fig. 4.

Conclusions

Peak picking and structure identification still remain the most significant challenging tasks in untargeted analytics. The statistical analysis and mass defect filters presented in this paper have demonstrated the capability to successfully filter thousands of m/z signals to 70 signals to be potential candidates to OFX TPs. The application of the *in-home* data scripts significantly reduced data processing time and allowed the automated detection of candidate TPs, even if some of them were coeluting or masked by the background noise. Although all these filtering parameters described can be easily defined and modified for instant results update, the mass spectrometrist's critical point of view is crucial to identify *in-source* reactions that might be taking place, inducing false data interpretation. In addition to classical structural elucidation techniques based on HRMS and MS/HRMS, the study of the isotope labelled ofloxacin OFX(-d_3), has proven to be of significant support for the correct structure assignment. Moreover, its use has also provided a deeper understanding on the mechanism involved in the photocatalytical process since it was possible to compare OFX(-d_3) kinetics. On the basis of the identified TPs and their observed kinetics, it was proposed a general scheme of degradation which started with little modifications of OFX structure such as reduction, oxidations, hydroxylations and ended with low molecular weight structures. High molecular weight structures were also detected, presumably corresponding to OFX dimers generated in the termination step of the radical processes. Furthermore, it has been possible to discriminate between first generation TPs and their consecutive transformation pattern. Finally, these results are the starting point of toxicological studies addressed to assess the potential toxicology of the characterised TPs.

Acknowledgements

J. Jimenez-Villarin thanks to Ms. Laura Meschede Anglada and Dr. Diego Morillo Martin from Leitat Technological Center for providing TiO_2 nanofibers and supported photocatalysts. The authors are gratefully acknowledged for the financial support of the Catalan Government under the project of industrial doctorate scholarship (2013 DI 044). The authors gratefully acknowledge the financial support by the Ministry of Science and Technology of the Spanish Government under the project CTQ2012-30836, and from the Agency for Administration of University and Research Grants (Generalitat de Catalunya, Spain) under the project 2014 SGR-539.

Appendix A. Supplementary data

Supplementary data associated with this article can be found, in the online version, at http://dx.doi.org/10.1016/j.chroma.2016.03.063.

References

[1] R. Jarboui, M. Chtourou, C. Azri, N. Gharsallah, E. Ammar, Time-dependent evolution of olive mill wastewater sludge organic and inorganic components and resident microbiota in multi-pond evaporation system, Bioresour. Technol. 101 (2010) 5749–5758.
[2] T. Paul, M.C. Dodd, T.J. Strathmann, Photolytic and photocatalytic decomposition of aqueous ciprofloxacin: transformation products and residual antibacterial activity, Water Res. 44 (2010) 3121–3132.
[3] M. Sleiman, C. Ferronato, B. Fenet, R. Baudot, F. Jaber, J.-M. Chovelon, Chovelon development of HPLC/ESI-MS and HPLC/^{1}H NMR methods for the identification of photocatalytic degradation products of iodosulfuron, Anal. Chem. 78 (2006) 2957–2966.
[4] X. Van Doorslaer, K. Demeestere, P.M. Heynderickx, M. Caussyn, H. Van Langenhove, F. Devlieghere, A. Vermeulen, J. Dewulf, Heterogeneous photocatalysis of moxifloxacin: identification of degradation products and determination of residual antibacterial activity, Appl. Catal. B—Environ. 138 (2013) 333–341.
[5] A. Fujishima, X. Zhang, D.A. Tryk, TiO_2 photocatalysis and related surface phenomena, Surf. Sci. Rep. 63 (2008) 515–582.
[6] P. Salvador, On the nature of photogenerated radical species active in the oxidative degradation of dissolved pollutants with TiO_2 aqueous suspensions: a revision in the light of the electronic structure of adsorbed water, J. Phys. Chem. C 111 (2007) 17038–17043.
[7] O. Legrini, E. Oliveros, A.M. Braun, Photochemical processes for water treatment, Chem. Rev. 93 (1993) 671–698.
[8] O. Carp, C.L. Huisman, A. Reller, Photoinduced reactivity of titanium dioxide, Prog. Solid State Chem. 32 (1-2) (2004) 33–177.
[9] K. Yoon, B.S. Hsiao, B. Chu, Functional nanofibers for environmental applications, J. Mater. Chem. 18 (2008) 5326–5334.
[10] Z. Liu, H. Bai, D.D. Sun, A general method for the fabrication of hierarchically-nanostructured membranes with multifunctional environmental applications, Sep. Purif. Technol. 107 (2013) 324–330.
[11] S.K. Choi, S. Kim, S.K. Lim, H. Park, Photocatalytic comparison of TiO_2 nanoparticles and electrospun TiO_2 nanofibers: effects of mesoporosity and interparticle charge transfer, J. Phys. Chem. C 114 (2010) 16475–16480.
[12] M. Grabenauer, W.L. Krol, J.L. Wiley, B.F. Thomas, Analysis of synthetic cannabinoids using high-resolution mass spectrometry and mass defect filtering: implications for nontargeted screening of designer drugs, Anal. Chem. 84 (2012) 5574–5581.
[13] F.C. Marhuenda-Egea, R.D. Gonsalvez-Alvarez, B. Lledo-Bosch, J. Ten, R. Bernabeu, New approach for chemometric analysis of mass spectrometry data, Anal. Chem. 85 (2013) 3053–3058.
[14] X. Liu, Z. Ser, J.W. Locasale, Development and quantitative evaluation of a high-resolution metabolomics technology, Anal. Chem. 86 (2014) 2175–2184.
[15] https://metlin.scripps.edu/index.php.
[16] http://www.massbank.jp.
[17] MZCloud, https://www.mzcloud.org/.
[18] T. Pluskal, T. Uehara, M. Yanagida, Highly accurate chemical formula prediction tool utilizing high-resolution mass spectra, MS/MS fragmentation heuristic rules, and isotope pattern matching, Anal. Chem. 84 (2012) 4396–4403.
[19] S. Wolf, S. Schmidt, M. Müller-Hannemann, S. Neumann, In silico fragmentation for computer assisted identification of metabolite mass spectra, BMC Bioinf. 11 (2010) 148.
[20] M. Gerlich, S. Neumann, MetFusion: integration of compound identification strategies, J. Mass Spectrom. 48 (2013) 291–298.
[21] F. Du, Q. Ruan, M. Zhu, J. Xing, Detection and characterization of ticlopidine conjugates in rat bile using high-resolution mass spectrometry: applications of various data acquisition and processing tools, J. Mass Spectrom. 48 (2013) 413–422.
[22] W. Lam, R. Ramanathan, In electrospray ionization source hydrogen/deuterium exchange LC–MS and LC–MS/MS for characterization of metabolites, J. Am. Soc. Mass Spectrom. 13 (2002) 345–353.
[23] A. Tolonen, M. Turpeinen, J. Uusitalo, O. Pelkonen, A simple method for differentiation of monoisotopic drug metabolites with hydrogen–deuterium exchange liquid chromatography/electrospray mass spectrometry, Eur. J. Pharm. Sci. 25 (2005) 155–162.
[24] N.K.N. Neumann, S.M. Lehner, B. Kluger, C. Bueschl, K. Sedelmaier, M. Lemmens, R. Krska, R. Schuhmacher, Automated LC-HRMS(/MS) approach for the annotation of fragment ions derived from stable isotope labeling-assisted untargeted metabolomics, Anal. Chem. 86 (2014) 7320–7327.
[25] P.M. Cano, E.L. Jamin, S. Tadrist, P. Bourdaud'hui, M. Péan, L. Debrauwer, I.P. Oswald, M. Delaforge, O. Puel, New untargeted metabolic profiling combining mass spectrometry and isotopic labeling: application on aspergillus fumigatus grown on wheat, Anal. Chem. 85 (2013) 8412–8420.
[26] P. Calza, C. Medana, F. Carbone, V. Giancotti, C. Baiocchi, Characterization of intermediate compounds formed upon photoinduced degradation of

quinolones by high-performance liquid chromatography/high-resolution multiple-stage mass spectrometry, Rapid Commun. Mass Spectrom. 22 (2008) 1533–1552.
[27] E. Hapeshi, A. Achilleos, M.I. Vasquez, C. Michael, N.P. Xekoukoulotakis, D. Mantzavinos, D. Kassinos, Drugs degrading photocatalytically: kinetics and mechanisms of ofloxacin and atenolol removal on titania suspensions, Water Res. 44 (2010) 1737–1746.
[28] I. Michael, E. Hapeshi, C. Michael, D.I. Fatta-Kassinos, E. Michael, C. Hapeshi, D. Michael, Fatta-Kassinos, solar Fenton and solar TiO_2 catalytic treatment of ofloxacin in secondary treated effluents: evaluation of operational and kinetic parameters, Water Res. 44 (2010) 5450–5462.
[29] E. Hapeshi, I. Fotiou, D. Fatta-Kassinos, Sonophotocatalytic treatment of ofloxacin in secondary treated effluent and elucidation of its transformation products, Chem. Eng. J. 224 (2013) 96–105.
[30] R. Vessecchi, A.E.M. Crotti, T. Guaratini, P. Colepicolo, S.E. Galembeck, N. Lopes, Radical ion generation processes of organic compounds in electrospray ionization mass spectrometry, Mini-Rev. Org. Chem. 4 (2007) 75–87.
[31] J. Genovino, S. Lütz, D. Sames, B.B. Touré, Complementation of biotransformations with chemical CH oxidation: copper-catalyzed oxidation of tertiary amines in complex pharmaceuticals, J. Am. Chem. Soc. 135 (2013) 12346–12352.
[32] N. Washida, H. Takagi, Reaction of cyclohexane and cyclohexyl radicals with atomic and molecular oxygen, J. Am. Chem. Soc. 104 (1982) 168–173.
[33] Y. Souissi, S. Bourcier, S. Ait-Aissa, E. Miallot-Maréchal, S. Bouchonnet, C. Genty, M. Sablier, Using mass spectrometry to highlight structures of degradation compounds obtained by photolysis of chloroacetamides: case of acetochlor, J. Chromatogr. A 1310 (2013) 98–112.
[34] J. Poerschmann, U. Trommler, T. Górecki, Aromatic intermediate formation during oxidative degradation of bisphenol A by homogeneous sub-stoichiometric Fenton reaction, Chemosphere 79 (2010) 975–986.
[35] K. Koci, L. Obalová, L. Matejova, D. Plachá, Z. Lacný, J. Jirkovský, O. Solcová, Effect of TiO_2 particle size on the photocatalytic reduction of CO_2, Appl. Catal. B: Environ. 89 (2009) 494–502.
[36] J. Lee, W. Choi, Effect of platinum deposits on TiO_2 on the anoxic photocatalytic degradation pathways of alkylamines in water: dealkylation and nalkyation, Environ. Sci. Technol. 38 (2004) 4026–4033.